

Topological Anderson Insulator in Three Dimensions

H.-M. Guo,^{1,2} G. Rosenberg,¹ G. Refael,³ and M. Franz¹

¹*Department of Physics and Astronomy, University of British Columbia, Vancouver, BC, Canada V6T 1Z1*

²*Department of Physics, Capital Normal University, Beijing 100048, China*

³*Department of Physics, California Institute of Technology, Pasadena, CA 91125*

(Dated: February 5, 2022)

When the spin-orbit coupling generates a band inversion in a narrow-bandgap semiconductor such as $\text{Sb}_x\text{Bi}_{1-x}$ or Bi_2Se_3 the resulting system becomes a strong topological insulator (STI)^{1,2}. A key defining property of a STI are its topologically protected metallic surface states. These are immune to the effects of non-magnetic disorder and form a basis for numerous theoretically predicted exotic phenomena^{3–7} as well as proposed practical applications^{8,9}. Disorder, ubiquitously present in solids, is normally detrimental to the stability of ordered states of matter. In this letter we demonstrate that not only is STI robust to disorder but, remarkably, under certain conditions disorder can become fundamentally responsible for its existence. We show that disorder, when sufficiently strong, can transform an ordinary metal with strong spin-orbit coupling into a strong topological ‘Anderson’ insulator, a new topological phase of quantum matter in three dimensions.

Disorder is well known to play a fundamental role in low-dimensional electronic systems, leading to electron localization and consequent insulating behavior in the time-reversal invariant systems¹⁰. Disorder also underlies much of the phenomenology of the integer quantum Hall effect¹¹. Recently, in a remarkable development, it has been noted first by numerical simulations¹² and shortly thereafter by analytical studies¹³, that a phase similar to the two dimensional topological insulator (also known as the quantum spin-Hall insulator^{14,15}) can be brought about by introducing non-magnetic disorder into a 2D metal with strong spin orbit coupling. This new 2D topological phase, referred to as topological Anderson insulator (TAI), has a disordered insulating bulk with topologically protected gapless edge states that give rise to precisely *quantized* conductance e^2/h per edge. In TAI, remarkably, conductance quantization owes its very existence to disorder.

A question naturally arises whether such behavior can occur in three spatial dimensions. More precisely, one may inquire whether an inherently 3D topological phase analogous to the *strong* topological insulator^{16–18} (STI) could be reached by disordering a clean system that is initially in a topologically trivial phase. This is a nontrivial question because just as the 3D STI cannot be reduced to the set of 2D topological insulators, the existence of a 3D ‘strong’ TAI presumably cannot be deduced from the physics of 2D TAI. Below, we show the answer to the

above question to be affirmative. Employing a combination of analytical and numerical methods we construct an explicit example of a disorder-induced topological phase in three dimensions with physical properties analogous to those of the strong topological insulator. We propose to call this new phase a ‘strong topological Anderson insulator’ (STAI). We argue that some of the topologically trivial compounds with strong spin-orbit coupling discussed in the recent literature, such as e.g. Sb_2Se_3 , could become STAI upon introducing disorder. In other compounds that already are STIs in their clean form, disorder can reinforce this behavior by rendering the bulk truly insulating. We note that the authors of Ref. [13] anticipated the existence of a 3D disorder-induced topological phase.

To study the emergence of the STAI we consider a variant of a model describing itinerant electrons with spin-orbit coupling on a cubic lattice discussed extensively in the recent literature^{4,19,20}. It has four electron states per lattice site \mathbf{r}_j , compactly denoted as $\Psi_j = (\psi_{1j}, \psi_{2j}, \psi_{3j}, \psi_{4j})^T$, and a momentum space Hamiltonian $H_0 = \sum_{\mathbf{k}} \Psi_{\mathbf{k}}^\dagger \mathcal{H}_{\mathbf{k}} \Psi_{\mathbf{k}}$ with $\Psi_{\mathbf{k}}$ the Fourier transform of Ψ_j ,

$$\mathcal{H}_{\mathbf{k}} = \sum_{\mu=0}^3 d_{\mu}(\mathbf{k}) \Gamma_{\mu} + d_4(\mathbf{k}) \mathbb{1}, \quad (1)$$

and $d_0(\mathbf{k}) = \epsilon - 2t \sum_i \cos k_i$, $d_i(\mathbf{k}) = -2\lambda \sin k_i$ ($i = 1, 2, 3$) and $d_4(\mathbf{k}) = 2\gamma \sum_i (1 - \cos k_i)$. Here Γ_{μ} are 4×4 Dirac matrices in combined orbital and spin space, satisfying the canonical anticommutation relation $\{\Gamma_{\mu}, \Gamma_{\nu}\} = 2\delta_{\mu\nu}$. The system defined by H_0 is invariant under time-reversal and spatial inversion. In the following we take two alternate points of view regarding Hamiltonian (1): (i) we view it as a simple toy model conveniently describing both topological and ordinary phases of non-interacting electrons in 3D and, (ii) we regard it as a lattice regularization of the effective low-energy Hamiltonian describing the physics of insulators in the Bi_2Se_3 family^{21–23}. In the latter interpretation Ψ_j labels the manifold of four active orbitals ($|P1_z^+, \uparrow\rangle, |P2_z^-, \uparrow\rangle, |P1_z^+, \downarrow\rangle, |P2_z^-, \downarrow\rangle$). In addition, parameters t, λ and γ in these materials show uniaxial anisotropy. We shall ignore this feature for now but return to it in our discussion of the physical realization of STAI.

The energy spectrum of H_0 has two doubly degenerate

bands,

$$E_{\mathbf{k}} = d_4(\mathbf{k}) \pm \sqrt{\sum_{\mu} d_{\mu}^2(\mathbf{k})}. \quad (2)$$

At half filling, depending on the values of the parameters ϵ , t , λ , and γ the system can be a metal, a trivial insulator, as well as a strong and weak topological insulator^{4,20}. Below, we focus on the topological phase transition between the ordinary insulator characterized by the Z_2 invariant^{16,17} (0;000) and the (1;000) STI phase. In the clean system modeled by Hamiltonian (1) this transition occurs due to the band inversion at the Γ -point of the Brillouin zone and can be driven by tuning parameter ϵ through a critical value $\epsilon_c = 6t$. We take t , λ and γ positive here and in what follows. We note that it is exactly this physics that underlies the STI behavior in the Bi_2Se_3 family of materials^{21–23}. Our main result is the finding that a similar transition can be effected by introducing non-magnetic disorder into a system that is topologically trivial in its clean form.

To simulate the effects of disorder we consider a Hamiltonian of the form

$$H = H_0 + \sum_j U_j \Psi_j^\dagger \Psi_j, \quad (3)$$

where H_0 is the disorder-free Hamiltonian discussed above and U_j is a random on-site potential uniformly distributed in the range $(-U_0/2, U_0/2)$. Following the discussion in Ref. [13] we start by treating the disorder within the self-consistent Born approximation (SCBA). The disorder-averaged electron propagator $g(\omega, \mathbf{k}) = (\omega + i\delta + E_F - \mathcal{H}_{\mathbf{k}} - \Sigma_{\mathbf{k}})^{-1}$ is then given in terms of disorder self-energy $\Sigma_{\mathbf{k}}$, subject to the self-consistent equation

$$\Sigma_{\mathbf{k}} = \frac{U_0^2}{12} \sum_{\mathbf{k} \in \text{BZ}} (E_F + i\delta - \mathcal{H}_{\mathbf{k}} - \Sigma_{\mathbf{k}})^{-1}. \quad (4)$$

Here E_F refers to the Fermi energy and δ is a positive infinitesimal. The factor of 12 arises from the variance $\langle U^2 \rangle = U_0^2/12$. General symmetry consideration restrict the form of the self-energy to $\Sigma_{\mathbf{k}} = \sum_{\mu} \Gamma_{\mu} \Sigma_{\mu}(\mathbf{k}) + \mathbb{1} \Sigma_4(\mathbf{k})$. In addition, for point-like disorder $\Sigma_{\mathbf{k}}$ is momentum independent. This forces $\Sigma_i(\mathbf{k})$ to vanish for $i = 1, 2, 3$ as any non-zero value would signal spontaneous time-reversal symmetry breaking caused by non-magnetic impurities.

The two non-vanishing components of the self-energy, Σ_0 and Σ_4 , can be viewed as disorder-induced renormalizations of the ‘topological mass’ $m \equiv d_0(\mathbf{k} = 0) = \epsilon - 6t$ and the Fermi energy E_F , respectively. Specifically, it is easy to see that within the SCBA the disorder-averaged system is described by the same propagator $g_0(\omega, \mathbf{k}) = (\omega + i\delta + E_F - \mathcal{H}_{\mathbf{k}})^{-1}$ as the clean system but with parameters m and E_F replaced as $m \rightarrow \bar{m} = m + \Sigma_0$ and $E_F \rightarrow \bar{E}_F = E_F - \Sigma_4$. We note that Σ_0 and Σ_4 are generally complex-valued, giving \bar{m} and \bar{E}_F both real

and imaginary parts. The latter reflect the quasiparticle lifetime broadening due to disorder.

These considerations underlie the physical picture behind the emergence of STAI. Starting from a clean ordinary insulator (characterized by $m > 0$) disorder can induce a band inversion by driving the real part of the renormalized mass \bar{m} negative. According to the standard classification of topological insulators²⁴ a band inversion at an odd number of time-reversal invariant momenta changes the Z_2 class of the material. If the renormalized Fermi energy \bar{E}_F lies within the gap the resulting effective medium is a STI.

It is easy to obtain the self-consistent equations for \bar{m} and \bar{E}_F from Eq. (4). These read

$$\bar{m} = m - \frac{U_0^2}{12} \sum_{\mathbf{k}} \frac{\bar{m} + tc_{\mathbf{k}}}{D_{\mathbf{k}}}, \quad (5)$$

$$\bar{E}_F = E_F + \frac{U_0^2}{12} \sum_{\mathbf{k}} \frac{\bar{E}_F - \gamma c_{\mathbf{k}}}{D_{\mathbf{k}}}, \quad (6)$$

with $D_{\mathbf{k}} = \lambda^2 s_{\mathbf{k}}^2 + (\bar{m} + tc_{\mathbf{k}})^2 - (\bar{E}_F - \gamma c_{\mathbf{k}})^2 + i\delta$ and $s_{\mathbf{k}}^2 = 4 \sum_i \sin^2 k_i$, $c_{\mathbf{k}} = 2 \sum_i (1 - \cos k_i)$. We shall present the full solution to these below. To gain some insight into the underlying physics it is useful to first study the approximate solution valid at weak disorder (small U_0) obtained by replacing \bar{m} and \bar{E}_F on the right hand side by their respective bare values. One then obtains

$$\bar{m} \simeq m - \frac{U_0^2}{24\pi} \frac{t}{t^2 - \gamma^2}, \quad (7)$$

$$\bar{E}_F \simeq E_F + \frac{U_0^2}{24\pi} \frac{\gamma}{t^2 - \gamma^2}, \quad (8)$$

where we kept only the leading divergent terms after expanding the integrand around the Γ point. We observe that for $t > \gamma$ disorder indeed renormalizes the mass term downward; for $U_0 > U_c \simeq [24\pi m(t^2 - \gamma^2)/t]^{1/2}$ band inversion occurs and one expects the system to become a STAI. We demonstrate below that this conclusion remains valid when Eqs. (5,6) are solved self-consistently, as well as in the numerical simulation of Hamiltonian (3).

The expression for the critical disorder strength U_c derived above suggests that a significant amount of disorder might be necessary to effect the band inversion in a real material. Since the Born approximation is expected to hold in the limit of weak disorder it is important to establish the stability of STAI phase by means of a complementary method. To this end we carry out exact numerical diagonalization studies of our model Hamiltonian (3). Generalizing the approach of Refs. [12,13,25] we study the emergence of topologically protected gapless surface states that are the defining feature of the strong topological insulator in 3D. In a disordered system it is not sufficient to establish the existence of gapless modes as these could be localized in space. Instead, one must seek extended states capable of carrying electrical current across the macroscopic sample. With this in mind

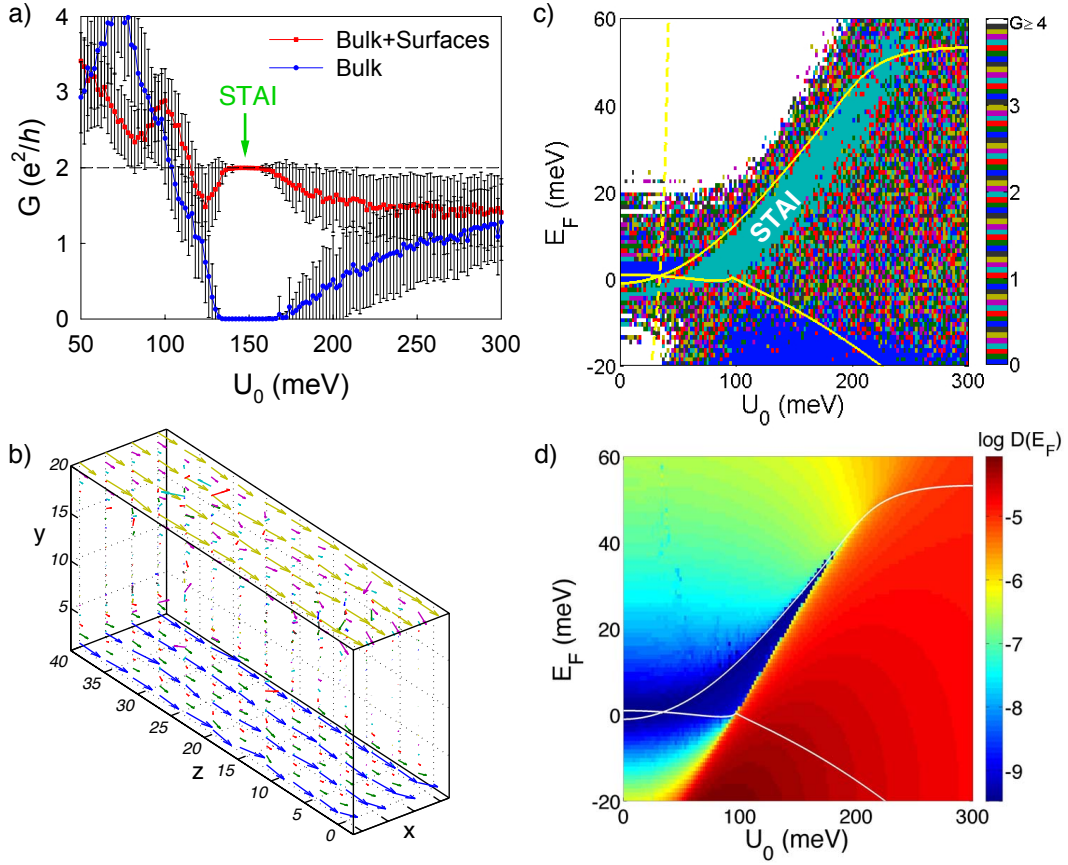


FIG. 1: **Conductance in disorder-induced phases.** a) Conductance G of a rectangular wire with dimensions $4 \times 20 \times 40$ as a function of disorder strength U_0 for periodic boundary conditions along x and periodic (open) boundary conditions along y as distinguished by blue (red) symbols, with $E_F = 20\text{meV}$. Error bars reflect the conductance fluctuations in the ensemble of 100 independent disorder realizations. b) Electrical current distribution in the STAI wire averaged over 100 independent disorder realization for $E_F = 20\text{meV}$ and $U_0 = 150\text{meV}$. We use open boundary conditions along y and periodic along x direction. Arrows representing the local current density in different layers along the y -direction have been color-coded for clarity. c) False color plot of conductance as a function of disorder strength U_0 and the Fermi energy E_F . Each data point corresponds to a single realization of the disorder potential. The color scale is chosen to emphasize the effect of fluctuations in G . The dashed line marks the band inversion boundary defined as $\text{Re}(\bar{m}) = 0$ based on the SCBA. Solid lines represent the SCBA phase boundaries separating a band insulator and a metal defined by $|\text{Re}(\bar{E}_F)| = |\text{Re}(\bar{m})|$. d) Density of states at the Fermi energy $D(E_F)$ calculated using SCBA. In all four panels we use parameters $\epsilon = 145\text{meV}$, $t = 24\text{meV}$, $\lambda = 20\text{meV}$, and $\gamma = 16\text{meV}$, corresponding to $m = 1\text{meV}$.

we employ the recursive Green's function method²⁶ to evaluate the conductance G of a length- L wire with a rectangular cross-section $W_x \times W_y$ using the Landauer-Büttiker formalism^{27,28}. For simplicity and concreteness, and to make contact with the previous works on 2D systems^{12,13,25}, we use model parameters listed in the caption of Fig. 1, with values close to those describing HgTe/CdTe quantum wells^{14,15}.

Figure 1a shows conductance G as a function of disorder strength U_0 in a wire with $W_x = 4$ and $W_y = 20$. For weak disorder the wire shows conductance characteristic of a disordered metal with significant fluctuations reflecting different realizations of the disorder potential U_i . Above $U_0 \simeq 130\text{meV}$ the bulk conductance (measured with periodic boundary conditions along x and y) drops to zero, indicating a disorder-induced insulating behav-

ior in the bulk that persists up to $U_0 \simeq 170\text{meV}$. If we change periodic boundary conditions to *open* along the y -direction a very different picture emerges. For U_0 in the range showing bulk insulating behavior the conductance is now pinned to the non-zero value $2e^2/h$ with no observable fluctuations. We attribute this to the ballistic transport of topologically protected surface states. Figure 1b confirms that the current flows near the surface only. It furthermore shows that the current density is equally distributed among the two surfaces; each surface forms an independent conduction channel contributing one quantum e^2/h to the total conductance G of the sample. This is the disorder-induced topological phase mentioned above.

How can one be sure that this is a genuinely 3D topological phase analogous to STI and not merely a result of

2D physics already discussed in Refs. [12,13]? First, we note that our model Hamiltonian is completely isotropic in 3D space so it is unlikely that the observed behavior would originate from the edge states of a set of 2D layers. We checked that the conductance remains quantized at $2e^2/h$ when we change the number of layers W_x and there is no even/odd effect that one would expect in a layered system. The odd number of 1D conductance channels per surface reflects the odd number of gapless states per surface of a STAI, confined to a 1D geometry imposed by the finite width of the wire in the x -direction. When we impose anti-periodic boundary conditions for the electron wavefunctions along the x -direction the conductance drops to zero in accord with the expectation for the surface state in a 3D topological phase.

To further confirm the 3D nature of the observed topological phase we probed for the Witten effect²⁹ in our model STAI. According to Refs. [4,5] the effective electromagnetic Lagrangian of a 3D strong topological insulator contains an unusual ‘axion’ term $\sim \theta \mathbf{E} \cdot \mathbf{B}$ with $\theta = \pi$. According to Witten²⁹ a magnetic monopole inserted into a medium with non-zero θ binds electric charge $-e(\theta/2\pi + n)$ with n integer. Using numerical methods described in Ref. [20] we measured the induced fractional charge in a configuration containing a monopole and an anti-monopole depicted in Fig. 2a. Our results presented in Fig. 2b,c clearly indicate fractional charge $\pm e/2$ bound to the monopole, confirming the expected value of $\theta = \pi$. This result lends additional support to our identification of STAI as a genuinely 3D topological phase characterized by the bulk axion term.

We now turn to the phase diagram of our model. Specifically, we wish to map out the locus of points in the space of parameters (E_F, U_0) that gives rise to STAI behavior. In a real material these parameters can be tuned, at least in principle, by adjusting the chemical composition and disorder content. Because of the 3D nature of our system and the resulting large size of the Hamiltonian matrix that must be diagonalized, we were able to consider only a single realization of the disorder potential U_i at each point of the (E_F, U_0) phase diagram. Nevertheless this turns out to be sufficient for determining the location of STAI phase to a good accuracy. Our method relies on the fact that, as seen in Fig. 1a, the conductance G shows no observable fluctuations in the STAI phase but fluctuates significantly elsewhere. Figure 1c displays G in a fashion that is designed to amplify the effect of fluctuations. The locus of STAI phase is clearly visible as the region with $G = 2e^2/h$ and no discernible conductance fluctuations.

The weak-disorder boundary of the numerically determined STAI phase coincides with the metal-insulator transition deduced from the SCBA Eqs. (7,8). As in 2D, the weak-disorder STAI phase boundary marks the crossing of a band edge rather than a mobility edge¹³. The strong-disorder phase boundary is more interesting. According to SCBA (Fig. 1d) states appear at the Fermi level beyond certain disorder strength $U^*(E_F)$ due to life-

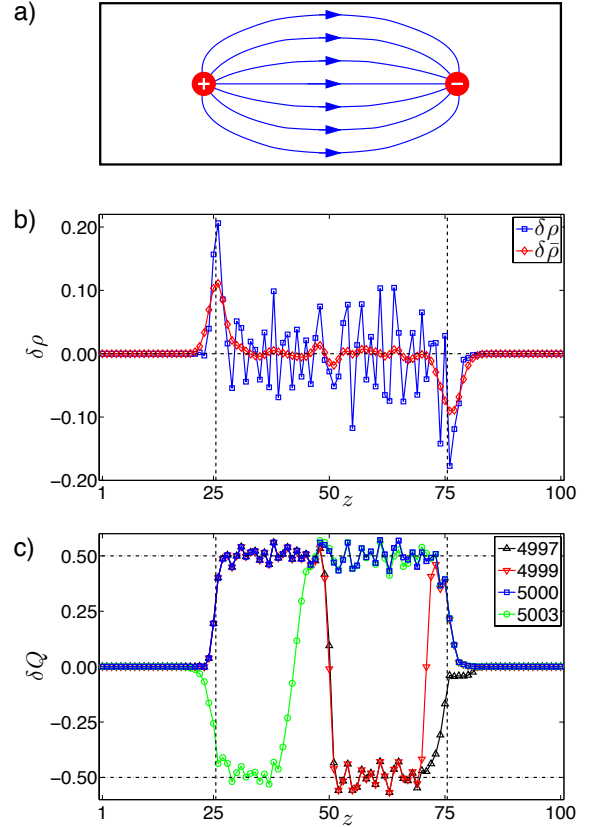


FIG. 2: Witten effect in the strong topological Anderson insulator. a) A prism-shaped sample with monopole (+), anti-monopole (-), and field lines indicated. The asymmetric field distribution allows us to use periodic boundary conditions in all directions and thus avoid difficulties associated with the surface states. b) Electric charge density $\delta\rho(z) = \sum_{x,y} [\rho(\mathbf{r}) - \rho_0(\mathbf{r})]$ induced by the monopole/anti-monopole pair in a $5 \times 5 \times 100$ sample at half filling. Here ρ and ρ_0 represent the charge density with and without the pair, respectively. A smoothed charge density function $\delta\bar{\rho}(z)$, obtained by convolving $\delta\rho(z)$ with a Gaussian of width $\sigma = 1.5$, is also plotted to emphasize charge bound to the monopole. c) Integrated charge $\delta Q(z) = \sum_{z' \leq z} \delta\rho(z')$ in units of e for E_F in the range 19 – 25 meV, corresponding to the STAI phase. The number of filled electron states is indicated in the legend (5000 represents the half-filling). The steps of magnitude $\pm e/2$ at the monopole/anti-monopole locations show the expected localized fractional charge due to the Witten effect. Steps with magnitude $\pm e$ located elsewhere are due to the shift of some bound states in applied magnetic field and can be viewed as a finite-size effect which should diminish for a system with a larger cross section. In both panels we use $U_0 = 150$ meV and other parameters as in Fig. 1.

time broadening. The band edge becomes ill-defined here as the self energy acquires a large imaginary part. Comparison to Fig. 1c shows that the numerically determined STAI phase extends well beyond $U^*(E_F)$. The bulk electron states near the Fermi level do not contribute to conduction in this regime and must therefore be localized. It is tempting to identify this region as the ‘true’ topologi-

cal Anderson insulator where electron localization plays the key role.

Although discussed here in the framework of a concrete model we expect the emergence of disorder-induced topological phases to be quite generic in three spatial dimensions. We have verified by an explicit calculation that including uniaxial anisotropy characteristic of the materials in the Bi_2Se_3 family²¹⁻²³ leads to qualitatively similar behavior to that displayed in Fig. 1. This suggests that clean Sb_2Se_3 , predicted to be a trivial insulator²¹ (but nevertheless close to the topological phase), could become STAI upon introducing non-magnetic disorder. Whether or not disorder can effect a band inversion in Sb_2Se_3 will depend crucially on the magnitude of its native bandgap. Our simulations suggest that when the bandgap size becomes larger than $\sim 20\text{meV}$ the amount of disorder required to produce

a band inversion is so large that the electron states become localized before STAI phase can be reached. From this point of view the best prospects for experimental realization of STAI physics lie with materials that are very-small or zero bandgap semiconductors with strong spin-orbit coupling. Although bulk HgTe as well as the recently discussed Heusler compounds^{30,31} exhibit this type of behavior their low-energy physics is not well described by our four-band model and further theoretical work is needed to determine whether disorder could drive the transition into the topological phase.

Acknowledgments — The authors acknowledge illuminating discussions with I. Garate, A. Kitaev, J.E. Moore, A. Vishwanath, C. Weeks and S.-C. Zhang. The work was supported in part by NSERC, CIFAR (MF), China Scholarship Council (HMG), the Packard Foundation, and the Research Corporation (GR).

-
- ¹ J.E. Moore, *Nature* **464**, 194 (2010).
 - ² M.Z. Hasan, C.L. Kane, arXiv:1002.3895.
 - ³ L. Fu and C.L. Kane, *Phys. Rev. Lett.* **100**, 096407 (2008).
 - ⁴ X.-L. Qi, T. Hughes, and S.-C. Zhang, *Phys. Rev. B* **78**, 195424 (2008).
 - ⁵ A.M. Essin, J.E. Moore, D. Vanderbilt, *Phys. Rev. Lett.* **102**, 146805 (2009).
 - ⁶ B. Seradjeh, J.E. Moore, and M. Franz, *Phys. Rev. Lett.* **103**, 066402 (2009).
 - ⁷ X. L. Qi *et al.*, *Science* **323**, 1184 (2009).
 - ⁸ T. Yokoyama, Y. Tanaka, and N. Nagaosa, *Phys. Rev. B* **81**, 121401(R) (2010).
 - ⁹ I. Garate and M. Franz, *Phys. Rev. Lett.* **104**, 146802 (2010).
 - ¹⁰ P.A. Lee and T.V. Ramakrishnan, *Rev. Mod. Phys.* **57**, 287 (1985).
 - ¹¹ F. Evers and A.D. Mirlin, *Rev. Mod. Phys.* **80**, 13551417 (2008).
 - ¹² J. Liu, R.-L. Chu, J.K. Jain and S.-Q. Shen, *Phys. Rev. Lett.* **102**, 136806 (2009).
 - ¹³ C.W. Groth, M. Wimmer, A.R. Akhmerov, J. Tworzydło and C.W.J. Beenakker, *Phys. Rev. Lett.* **103**, 196805 (2009).
 - ¹⁴ B.A. Bernevig, T.L. Hughes, and S.-C. Zhang, *Science* **314**, 1757 (2006).
 - ¹⁵ M. König *et al.*, *Science* **318**, 766 (2007).
 - ¹⁶ L. Fu, C. L. Kane, and E. J. Mele, *Phys. Rev. Lett.* **98**, 106803 (2007).
 - ¹⁷ J. E. Moore and L. Balents, *Phys. Rev. B* **75**, 121306(R) (2007).
 - ¹⁸ R. Roy, *Phys. Rev. B* **79**, 195322 (2009).
 - ¹⁹ P. Hosur, S. Ryu, and A. Vishwanath, *Phys. Rev. B* **81**, 045120 (2010).
 - ²⁰ G. Rosenberg and M. Franz, *Phys. Rev. B* (in press, arXiv:1001.3179).
 - ²¹ H. Zhang, C.-X. Liu, X.-L. Qi, X. Dai, Z. Fang, and S.-C. Zhang, *Nature Phys.* **5**, 438 (2009).
 - ²² Xia, Y. *et al.* *Nature Phys.* **5**, 398402 (2009).
 - ²³ Chen, Y.L. *et al.* *Science* **325**, 178181 (2009).
 - ²⁴ L. Fu and C. L. Kane, *Phys. Rev. B* **76**, 045302 (2007).
 - ²⁵ H. Jiang, L. Wang, Q.-F. Sun and X.C. Xie, *Phys. Rev. B* **80**, 165316 (2009).
 - ²⁶ We use the variant of the method described by G. Metalidis and P. Bruno, *Phys. Rev. B* **72**, 235304 (2005).
 - ²⁷ R. Landauer, *Philos. Mag.* **21**, 863 (1970).
 - ²⁸ M. Büttiker, *Phys. Rev. B* **38**, 9375 (1988).
 - ²⁹ E. Witten, *Phys. Lett. B* **86**, 283 (1979).
 - ³⁰ S. Chadov *et al.*, *Nature Mat.* (in press, arXiv:1003.0193).
 - ³¹ H. Lin *et al.*, *Nature Mat.* (in press, arXiv:1003.0155).